Chinese Chemical Letters 33 (2022) 3577–3580

Contents lists available at ScienceDirect

Chinese Chemical Letters

journal homepage: www.elsevier.com/locate/cclet

Synergy of photocatalytic reduction and adsorption for boosting uranium removal with PMo_{12}/UiO-66 heterojunction

Zhibin Zhang[a,b,1], Zifan Li[a,b,1], Zhimin Dong[a,b], Fengtao Yu[a,b], Yingcai Wang[a,b], Youqun Wang[a,b], Xiaohong Cao[a,b], Yuhui Liu[a,b,*], Yunhai Liu[a,b,*]

[a] Jiangxi Province Key Laboratory of Synthetic Chemistry, East China University of Technology, Nanchang 330013, China
[b] State Key Laboratory of Nuclear Resources and Environment, East China University of Technology, Nanchang 330013, China

ARTICLE INFO

Article history:
Received 21 November 2021
Revised 21 January 2022
Accepted 24 January 2022
Available online 31 January 2022

Keywords:
UiO-66
PMo12
Uranium
Adsorption
Photocatalytic reduction

ABSTRACT

In this work, we proposed a new U(VI) removal strategy combining adsorption and photocatalytic reduction by the PMo_{12}/UiO-66 heterojunctions. The PMo_{12} has been encapsulated in the cavities of UiO-66 by a one-step hydrothermal method, and the PMo_{12}/UiO-66 exhibited high adsorption capacity and photocatalytic activity. The maximal theoretical sorption capacity of U(VI) on 15% PMo_{12}/UiO-66 reached 225.36 mg/g and the photoreduction rate of 15% PMo_{12}/UiO-66 is about thirty times as much as UiO-66. Under the light irradiation, the photogenerated electrons rapidly transport from UiO-66 to PMo_{12}, and the photo-generated electrons could efficiently reduce the pre-enriched U(VI) to U(IV). This work provides new insights into remediation of the radioactive environment.

Developing nuclear power that has been exploited extensively as a clean energy source is of great significance to meet growing global energy demand [1]. As the fundamental elements of nuclear fuel, uranium possesses chemotoxicity and radiotoxicity, which can pose serious threats to the living organisms and natural environment [2]. Therefore, it is desirable to explore an effective and economical strategy for the removal of uranium [3].

Over the past few years, numerous adsorbents have been extensively investigated for removing uranium because of environment-friendly, convenient operation and high efficiency [4,5]. However, the adsorption capacity is preponderantly limited by the adsorption active sites, adsorption equilibrium between sorbent and solution, and available surface area [6]. Recently, the reduction of highly soluble U(VI) to insoluble U(IV) species by semiconductor photocatalyst has been extensively investigated [7,8]. The prior photocatalysis process of U(VI) reduction commonly contain the enriched of U(VI) on the surface of photocatalysts [9]. Feng *et al.* have been proved the adsorption of U(VI) was a vital step in photoreduction of U(VI) [10]. Considering the benefits of adsorption and the characteristics of uranium, integrating the adsorption and photocatalysis seems a more effective strategy for removing uranium. Chen *et al.* reported that the adsorbent-semiconductor hybrid nanosheet (g-C_3N_4/GO) composites exhibited high uranium removal capacity [11].

Polyoxometalates (POMs), a type of metal oxide nanoclusters, have been investigated for incorporating uranium atoms in polyoxometalate for the sequestration and storage of radioactive waste since early 1990s [12]. Besides, POMs are extensively used as catalysts due to the remarkable capability to receive electrons and redox properties [13]. However, the low surface area (1–10 m^2/g) and high solubility restricted the direct application of POMs. Therefore, MOFs have been selected as the matrix to encapsulate the POMs or employed organic linkages to graft MOFs and POMs together [14].

$[Zr_6O_4(OH)_4]$ clusters interlinked with twelve terephthalate ligands create one centrical octahedral cage (free diameters of 11 Å) and eight corner tetrahedral cages (8 Å) in each UiO-66 unit. The centrical octahedral cage provides an appropriate space for encapsulating PMo_{12} (~10 Å), and the stable structure of UiO-66 make the encapsulation of PMo_{12} be more reliable [15].

Herein, the PMo_{12}/UiO-66 has been assembled synthesized by a one-pot method and applied for the extraction of uranium. The prepared PMo_{12}/UiO-66 could effectively improve the adsorption capacity and the visible-light photocatalytic activity, which provides a new insight strategy for combined adsorption and photocatalytic reduction of uranyl ions.

The UiO-66 was synthesized according to the hydrothermal method [16]. The synthesis of PMo_{12}/UiO-66 was performed ac-

* Corresponding author at: State Key Laboratory of Nuclear Resources and Environment, East China University of Technology, Nanchang 330013, China.
E-mail addresses: liuyuhui@ecut.edu.cn (Y. Liu), yhliu@ecut.edu.cn (Y. Liu).
[1] These authors are contributed equally to this work.

https://doi.org/10.1016/j.cclet.2022.01.062
1001-8417/

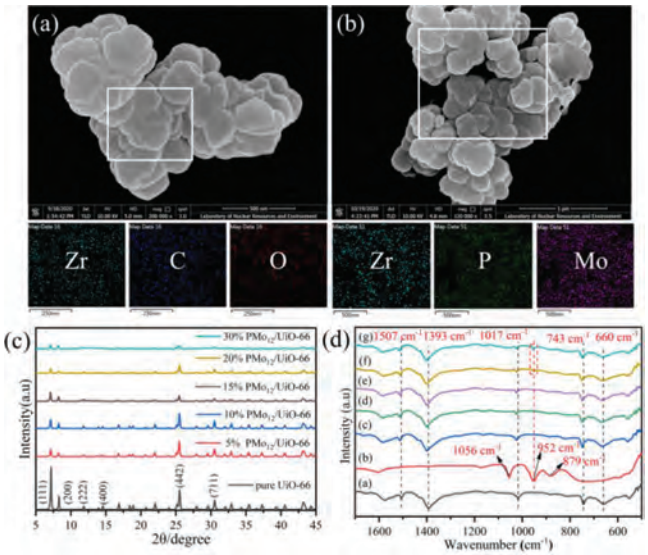

Fig. 1. SEM images and EDS elemental mapping images of pure UiO-66 (a) and 15% PMo_{12}/UiO-66 (b). (c) XRD patterns of the synthetic PMo_{12}/UiO-66 composites. (d) FT-IR spectra of the synthetic PMo_{12}/UiO-66 composites. Samples of (a, b) are UiO-66 and PMo_{12}. Samples of (c-g) are 5% PMo_{12}/UiO-66, 10% PMo_{12}/UiO-66, 15% PMo_{12}/UiO-66, 20% PMo_{12}/UiO-66, 30% PMo_{12}/UiO-66, respectively,.

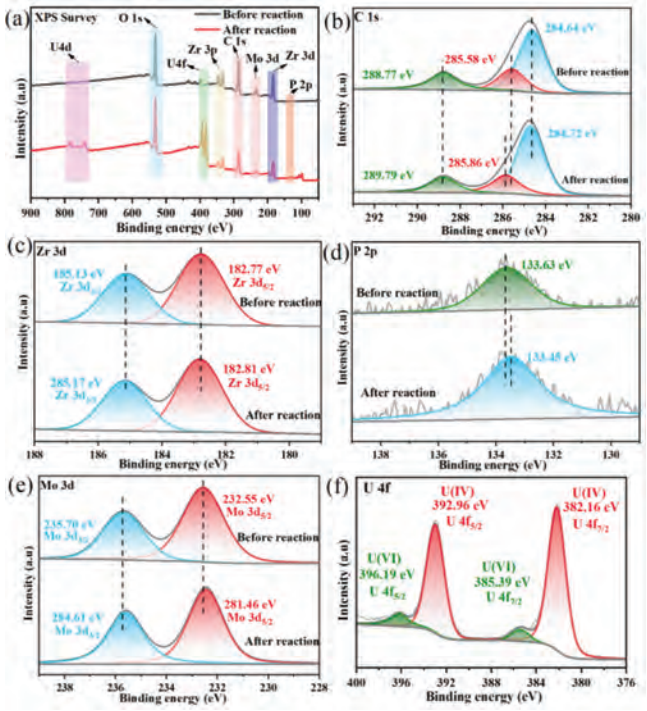

Fig. 2. XPS spectra of 15% PMo_{12}/UiO-66 before and after photoreaction: (a) Survey spectra; (b) C 1s; (c) Zr 3d; (d) P 2p; (e) Mo 3d; (f) U 4f.

cording to previous method with some modification [17]. Specifically, 1.1652 g zirconium chloride ($ZrCl_4$), 0.835 g terephthalic acid (BDC), 3.6 mL condensed HCl, and the required amount of PMo_{12} (5% PMo_{12} (0.1053 g), 10% PMo_{12} (0.2220 g), 15% PMo_{12} (0.3529 g), 20% PMo_{12} (0.500 g), 30% PMo_{12} (0.8591 g)) were added in DMF (40 mL). The resulting reaction mixture was ultrasonicated for ~30 min at room temperature. Then, the obtained mixtures were sealed in a Teflon-lined autoclave and kept in an oven at 120 °C for 24 h. The product was collected *via* centrifugation and washed for three times with DMF and methanol and then dried under vacuum at 60 °C. The obtained PMo_{12}/UiO-66 were named as X PMo_{12}/UiO-66, where X refer to 5%, 10%, 15%, 20% and 30% PMo_{12}. The characterization, photocatalytic tests and sorption experiments are described in Supporting information, respectively.

The morphology and microstructure of UiO-66 and 15% PMo_{12}/UiO-66 were investigated by scanning electron microscopy (SEM). According to Figs. 1a and b, the irregular octahedral UiO-66 about 300 nm with Zr, C, O elements dispersed uniformly can be observed, whereas the additional Mo and P elements can be found in 15% PMo_{12}/UiO-66, confirming the well dispersion of PMo_{12} nanoparticles in UiO-66 (Fig. S1 in Supporting information). The crystalline structures of UiO-66 and PMo_{12}/UiO-66 were confirmed by XRD (Fig. 1c). The diffraction peaks at 2θ of 7.15°, 8.30°, 11.83°, 14.57°, 25.52°, 30.53° and 42.94° correspond to the (111), (200), (220), (400), (442), and (711) crystal planes of UiO-66 [18]. For PMo_{12}/UiO-66, the peak intensities of UiO-66 gradually decreased with increasing the addition of PMo_{12}. However, no diffraction peaks of PMo_{12} can be observed in the PMo_{12}/UiO-66 probably due to the following two reasons: (1) the particle size of PMo_{12} clusters are relatively small (~10 Å); (2) the PMo_{12} clusters have been encapsulated in the cavities of UiO-66. Similar results can also be observed in the previous reports [19].

FI-IR spectra were investigated to recognize the functional groups on the surface of bare UiO-66, commercial PMo_{12} and PMo_{12}/UiO-66 (Fig. 1d). Two bands located at 660 cm^{-1} and 743 cm^{-1} correspond to the asymmetric stretching of C–H and C=C. The bands at 1017 cm^{-1} and 1393 cm^{-1} are the signals of Zr–O and O=C=O symmetric stretching, while the weak band at 1507 cm^{-1} represents the C=C of benzene ring [20]. Three characteristic peaks are observed for PMo_{12} at 1056 cm^{-1}, 952 cm^{-1}, 879 cm^{-1} attribute to the stretching vibrations of P–O, M=O and Mo–O–Mo, respectively [18]. Note that increasing the content of PMo_{12} causes a red shift for the vibration peaks of UiO-66. Furthermore, a new stretching vibration of M=O can be observed in 20% PMo_{12}/UiO-66 and 30% PMo_{12}/UiO-66 owing to the incorporation of PMo_{12}. The TG analyses have also confirmed it (Fig. S2 in Supporting information).

The chemical composition and chemical state of as prepared samples were investigated by XPS. The survey spectra revealed the presence of Zr, C, O, Mo, P in the 15% PMo_{12}/UiO-66, which are consistent with EDS analysis (Fig. 2a). The peaks at 284.64 eV, 285.58, and 288.77 eV are indexed to the binding energies of C–C, C–O and O–C=O [21], while the peaks at 182.77 eV and 185.13 eV are referring to Zr $3d_{5/2}$ and $3d_{3/2}$ in the high-resolution XPS C 1s and Zr 3d spectra of UiO-66 (Figs. 2b and c) [22]. In addition, the peaks at 232.55 eV and 235.70 eV are ascribed to Mo $3d_{5/2}$ and $3d_{3/2}$ (Fig. 2e) [23], whereas the framed peak at 133.63 eV is due to the deconvoluted P 2p spectra, revealing the P^{5+} state in PMo_{12}/UiO-66 (Fig. 2d) [24].

Fig. 3a shows the adsorption dynamics process of U(VI) onto UiO-66 and 15% PMo_{12}/UiO-66 in the darkness at pH 5.5. The adsorption rate is comparatively rapid during the first 50 min and then gradually becomes slowly after 100 min causing by the occupied and decreased active sites. Obviously, the adsorption process is well fitted with *pseudo*-second-order model with the values of R^2 near 1.0 (Table S1 in Supporting information). The q_e values derived from the *pseudo*-second-order model are 140.83 mg/g (15% PMo_{12}/UiO-66) and 53.58 mg/g (UiO-66) which are close to the experimental capacities of 15% PMo_{12}/UiO-66 (131.37 mg/g) and UiO-66 (52.13 mg/g), confirming that the uptake processes of uranyl ions are relied on the assumption of the rate-limiting chemical process rather than mass transport. Furthermore, the surface charge of 15% PMo_{12}/UiO-66 is more negative than that of UiO-66 due to the existence of PMo_{12} (Fig. S3 in Supporting information). The species of U(VI) are primarily existing as UO_2^{2+} at pH

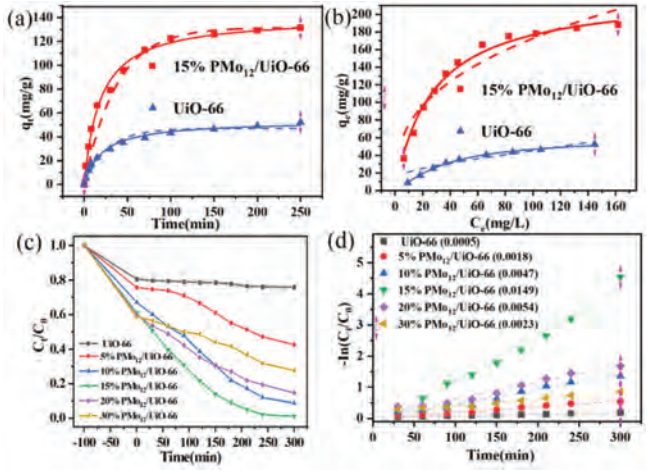

Fig. 3. (a) The sorption kinetics of UiO-66 and 15% PMo_{12}/UiO-66, the full lines and dotted lines are non-linear *pseudo*-first-order and *pseudo*-second-order kinetics model, respectively; (b) The sorption isotherms of UiO-66 and 15% PMo_{12}/UiO-66. The full lines and dotted lines are Langmuir and Freundlich adsorption isotherm models, respectively; (c) Photocatalytic reduction by different samples; (d) The calculated first-order kinetics rate constant for the photocatalytic reaction.

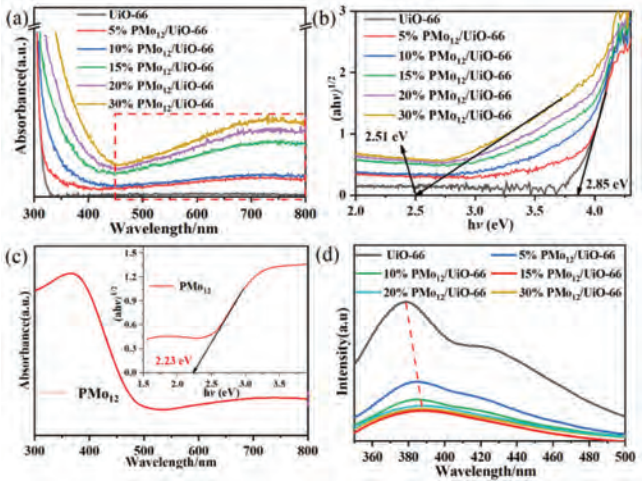

Fig. 4. (a) UV–vis diffuse reflectance spectra of as-prepared samples; (b) Tauc plot band gap estimation from UV–vis diffuse reflectance spectra of samples; (c) UV–vis diffuse reflectance spectra of PMo_{12}; (inset) Tauc plot band gap; (d) PL emission spectra of as-prepared samples.

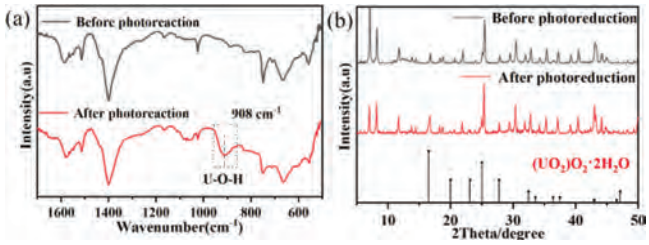

Fig. 5. FT-IR (a) and XRD (b) patterns of 15% PMo_{12}/UiO-66 before and after photoreaction.

5.5, thereby the charge attraction between cationic UO_2^{2+} with PMo_{12}/UiO-66 could boost the surface adsorption.

The adsorption isotherms of UiO-66 and 15% PMo_{12}/UiO-66 are revealed Fig. 3b. Clearly, the correlation coefficients ($R^2 > 0.98$) of Langmuir model are much higher than that of Freundlich model ($R^2 = 0.85$–0.96) (Table S2 in Supporting information), demonstrating that the dominant adsorption process was monolayer adsorption. The fitted maximum U(VI) uptake capacity of 15% PMo_{12}/UiO-66 was calculated to be 225.36 mg/g according to Langmuir model, which is much larger than that of UiO-66 (59.67 mg/g). More importantly, the adsorbed U(VI) on the surface of PMo_{12}/UiO-66 could boost the transfer of excited electrons [25,26].

The photocatalytic reduction of U(VI) was tested under 300 W Xe lamp irradiation, and the results are shown in Fig. 3c. The pure UiO-66 has low photocatalytic activity due to the rapid recombination of charge carriers and limited light absorption range. Comparatively, the 15% PMo_{12}/UiO-66 shows the best photoreduction activity and the total removal efficiency reaches 98.92% within 300 min irradiation, and the U(VI) photoreduction rate attains 0.0149 min^{-1}, about thirty times as much as UiO-66 (0.0005 min^{-1}) (Fig. 3d).

It can be seen from the UV–vis absorption spectra (Fig. 4a) that the PMo_{12}/UiO-66 heterojunctions display enhanced visible-light harvesting in the range of 450–800 nm owing to the competitive absorption factor of PMo_{12} cocatalyst (Fig. 4a). The corresponding Tauc plot shows the band gap of UiO-66 and PMo_{12} are 2.85 eV and 2.23 eV, respectively (Figs. 4b and c). The intensity of photoluminescence (PL) spectra can reflect the extent of recombination of the photo-generated charges. As shown in Fig. 4d, the pristine UiO-66 displays striking emission peaks at 380 nm, in contrast, the fluorescence of PMo_{12}/UiO-66 heterojunctions are partially quenched due to the formation of heterojunction between UiO-66 and PMo_{12}. The 15% PMo_{12}/UiO-66 shows the lowest PL peak intensity, suggesting that it has the most efficient suppression for charge recombination. The relationship between light harvesting and charges separation is currently conflicting, and the 15% PMo_{12}/UiO-66 achieves the optimum point [27].

As displayed in Fig. S4 (Supporting information), the Mott-Schottky curves of UiO-66 show a positive slope, indicating the characteristics of n-type semiconductors. The flat band potential of UiO-66 is −0.70 V *vs.* Ag/AgCl. The conduction band (CB) edge nearly overlaps the flat band potential [28], thus, the CB of UiO-66 is calculated to be −0.50 V *vs.* NHE. Moreover, the flat-band potential of PMo_{12} is around −0.28 V *vs.* NHE [19]. The CB position of UiO-66 is lower than that of PMo_{12}, which means the electrons on the UiO-66 can be smoothly transferred to the PMo_{12} due to E_f equilibrium in the PMo_{12}/UiO-66 heterojunction. As described in Fig. 2, the chemical environment of C, Zr, Mo and P have changed after photoreaction. Specifically, the peaks of C and Zr red shift by 0.08 eV and 0.04 eV, whereas the peaks of P and Mo blue shift by 0.18 eV and 0.09 eV. The above offsets of peaks indicate that the electrons migrate from UiO-66 to PMo_{12}, confirming the formation of heterojunction [29]. Additionally, in the U 4f spectra of 15% PMo_{12}/UiO-66, four peaks at 396.19 eV, 395.39 eV and 392.96 eV, 382.16 eV are attributed to U(VI) and U(IV), indicating the coexistence of U(VI) and U(IV) species (Fig. 2f) [30]. In Fig. 5a the new vibration band at 899 cm^{-1} is the asymmetric stretching of uranyl species [31], and have been confirmed as uranium peroxide, $(UO_2)O_2{\cdot}2H_2O$ by XRD (Fig. 5b and Fig. S5 in Supporting information) [32]. The quenching experiments were conducted to verify the primary active substances involved in the photoreduction process in order to gain deeper insight into reaction mechanism (Fig. S6 in Supporting information). The photocatalytic activity of 15% PMo_{12}/UiO-66 was inhibited after adding *p*-BQ, revealing that $\cdot O_2^-$ radicals are the main reduction radicals. In contrast, methanol acting as the hole scavenger can promote the separation of photoinduced carriers and improve the photocatalytic reduction, whereas the TBA shows no effect on the photoreaction, indicating $\cdot$OH radicals are unnecessary during the photoreaction. In conclusion, the removal of U(VI) by PMo_{12}/UiO-66 can be divided as follow steps: (i) The dissociative U(VI) ions were adsorbed on the surface of PMo_{12}/UiO-66 before photoreaction (Eq. 1). (ii) Under irra-

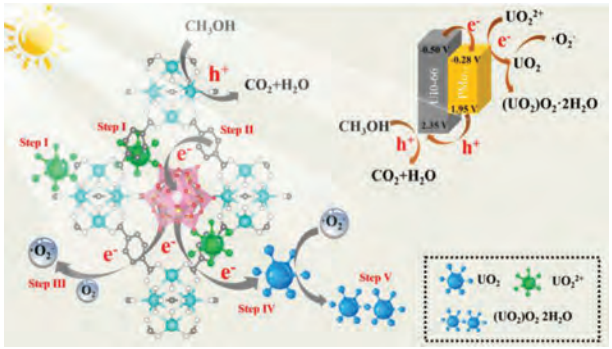

Fig. 6. The proposed mechanism for photocatalytic reduction uranium by 15% PMo_{12}/UiO-66 under visible-light illumination.

diation, the electrons in the CB of UiO-66 drift rapidly along the direction of the internal electric field to the CB of PMo_{12}, and reduce U(VI) pre-enriched in PMo_{12}/UiO-66 (Eq. 2). (iii) The U(VI) species were reduced by photoelectrons and $\cdot O_2^-$ radicals to form $(UO_2)O_2{\cdot}2H_2O$ (Eqs. 3–5) (Fig. 6).

$$PMo_{12}/UiO\text{-}66 + U(VI) \rightarrow U(VI)/PMo_{12}/UiO\text{-}66 \quad (1)$$

$$UiO\text{-}66\left(e^-\right) + PMo_{12} \rightarrow PMo_{12}\left(e^-\right) + UiO\text{-}66 \quad (2)$$

$$O_2 + PMo_{12}\left(e^-\right) \rightarrow \cdot O_2^- \quad (3)$$

$$UO_2^{2+} + PMo_{12}\left(e^-\right) \rightarrow UO_2(s) \quad (4)$$

$$UO_2(s) + \cdot O_2^- + 4H^+ \rightarrow (UO_2)O_2 \cdot 2H_2O \quad (5)$$

In summary, this work provides a new uranium removal strategy combining adsorption and photocatalysis. The encapsulation of PMo_{12} in UiO-66 could enhance the adsorption capacity to 225.36 mg/g. The PMo_{12} can also accept electrons transporting from UiO-66, and further reduce the U(VI) pre-enriched on the surface of PMo_{12}/UiO-66 heterojunctions. The reduced uranium specie was confirmed to be $(UO_2)O_2{\cdot}2H_2O$ due to the photoelectrons and $\cdot O_2^-$ radicals. Thus, there are reasons to believe that PMo_{12}/UiO-66 is a promising candidate for uranium extraction from radioactive wastewater.

Declaration of competing interest

The authors declare that they have no competing financial interests or personal relationships that could have appeared to influence the work reported in this paper.

Acknowledgments

This work was financially supported by the National Natural Science Foundation of China (Nos. 21866004, 21866003, 22066003, 22076022, 22006004), the Defense Industrial Technology Development Program (No. JCKY2019401C004), the Open Fund of Jiangxi Province Key Laboratory of Synthetic Chemistry (No. JXSC202012), the Open Fund of State Key Laboratory of Nuclear Resources and Environment (No. NRE1924), the Graduate Innovation Fund of East China University of Technology (No. DHYC-202134).

Supplementary materials

Supplementary material associated with this article can be found, in the online version, at doi:10.1016/j.cclet.2022.01.062.

References

[1] Z. Dong, Z. Zhang, R. Zhou, et al., Chem. Eng. J. 386 (2020) 123944.
[2] Z. Zhang, C. Liu, Z. Dong, et al., Appl. Surf. Sci. 520 (2020) 146352.
[3] K. Yu, P. Jiang, J. Wei, H. Yuan, Y. Xin, et al., J Hazard Mater. (2021) 127823.
[4] Z. Zhang, Z. Dong, X. Wang, et al., Chem. Eng. J. 370 (2019) 1376–1387.
[5] Z. Zhang, Z. Dong, X. Wang, et al., Chem. Eng. J. 341 (2018) 208–217.
[6] H. Li, F. Zhai, D. Gui, et al., Appl. Catal. B 254 (2019) 47–54.
[7] F. Yu, Z. Zhu, S. Wang, et al., Chem. Eng. J. 412 (2021) 127558.
[8] K. Yu, P. Jiang, H. Yuan, et al., Appl. Catal. B 288 (2021) 119978.
[9] H. Liu, J. Lei, J. Chen, et al., Nano Res. (2021) 1–9.
[10] J. Feng, Z. Yang, S. He, et al., Chemosphere 212 (2018) 114–123.
[11] T. Chen, J. Zhang, H. Ge, et al., J. Hazard. Mater. 384 (2020) 121383.
[12] H. Zhang, W. Liu, A. Li, et al., Angew. Chem. Int. Ed. 58 (2019) 16110–16114.
[13] M. Zhang, A.M. Zhang, X. Wang, et al., J. Mater. Chem. A 6 (2018) 8735–8741.
[14] Y. Huang, R. Wang, J. Mater. Chem. A 7 (2019) 12105–12114.
[15] X. Zhang, Z. Zhang, B. Zhang, et al., Appl. Catal. B 256 (2019) 117804.
[16] M.J. Katz, Z.J. Brown, Y.J. Colon, et al., Chem. Commun. 49 (2013) 9449–9451.
[17] R. Abazari, L. Esrafili, A. Morsali, Y. Wu, J. Gao, Appl. Catal. B 283 (2021) 119582.
[18] X. Chang, X.F. Yang, Y. Qiao, et al., Small 16 (2020) 1906432.
[19] R. Liang, R. Chen, F. Jing, N. Qin, L. Wu, Dalton Trans. 44 (2015) 18227–18236.
[20] R. Bariki, D. Majhi, K. Das, A. Behera, B.G. Mishra, Appl. Catal. B 270 (2020) 118882.
[21] F. Yang, S. Xie, G. Wang, et al., Environ. Sci. Pollut. Res. Int. 27 (2020) 20246–20258.
[22] X. Xie, X. Dao, F. Guo, et al., ChemistrySelect 5 (2020) 4001–4007.
[23] D. Hu, X. Song, S. Wu, et al., Chin. J. Catal. 42 (2021) 356–366.
[24] H. Shi, Y. Yu, Y. Zhang, et al., Appl. Catal. B 221 (2018) 280–289.
[25] K. Yu, P. Shao, P. Meng, et al., J. Hazard. Mater. 392 (2020) 122350.
[26] J. Lei, H. Liu, C. Yuan, et al., Chem. Eng. J. 416 (2021) 129164.
[27] Z. Li, Z. Zhang, Z. Dong, et al., Sep. Purif. Technol. 283 (2022) 120195.
[28] Y. Zhang, Z. Jin, Phys. Chem. Chem. Phys. 21 (2019) 8326–8341.
[29] Y. Zhang, M. Zhu, S. Zhang, et al., Appl. Catal. B 279 (2020) 119390.
[30] Z. Li, Z. Zhang, Z. Dong, et al., J. Solid. State. Chem. 303 (2021) 122499.
[31] Z. Li, Z. Zhang, Z. Dong, et al., J. Solid. State. Chem. 302 (2021) 122305.
[32] Z. Dong, Z. Zhang, Z. Li, et al., Environ. Sci. 8 (2021) 2372–2385.